

A Stabilization of a Continuous Limit of the Ensemble Kalman Filter

Dieter Armbruster

*School of Mathematical and Statistical Sciences
Arizona State University
Tempe, AZ 85287-1804, USA*

Michael Herty

*Institut für Geometrie und Praktische Mathematik (IGPM)
RWTH Aachen University
Templergraben 55, 52062 Aachen, Germany*

Giuseppe Visconti

*Institut für Geometrie und Praktische Mathematik (IGPM)
RWTH Aachen University
Templergraben 55, 52062 Aachen, Germany*

November 27, 2021

Abstract

The ensemble Kalman filter belongs to the class of iterative particle filtering methods and can be used for solving control-to-observable inverse problems. In recent years several continuous limits in the number of iteration and particles have been performed in order to study properties of the method. In particular, a one-dimensional linear stability analysis reveals a possible instability of the solution provided by the continuous-time limit of the ensemble Kalman filter for inverse problems. In this work we address this issue by introducing a stabilization of the dynamics which leads to a method with globally asymptotically stable solutions. We illustrate the performance of the stabilized version of the ensemble Kalman filter by using test inverse problems from the literature and comparing it with the classical formulation of the method.

Mathematics Subject Classification (2010) 37N35 (Dynamical systems in control), 65N21 (Inverse problems), 93E11 (Filtering)

Keywords Dynamical systems, inverse problems, regularization, stabilization, nonlinear filtering methods, moment equations

1 Introduction

In this paper we investigate a particular numerical method for solving inverse problems, namely, the Ensemble Kalman Filter (EnKF). While this method has already been introduced more than ten years ago [10] as a discrete time method to estimate state variables and parameters of stochastic dynamical systems, it has also been successfully applied to inverse problems [18]. In this context is also known as ensemble Kalman inversion. The EnKF is applied in many research fields due to its derivative-free structure, in particular in oceanography [11], reservoir modeling [1], weather forecasting [19], milling process [24], process control [25], and also machine learning [15, 20].

In order to set up the mathematical formulation, we let $\mathcal{G} : X \rightarrow Y$ be the given (possibly nonlinear) forward operator between finite dimensional Hilbert spaces $X = \mathbb{R}^d$, $d \in \mathbb{N}$, and $Y = \mathbb{R}^K$, $K \in \mathbb{N}$. We are concerned with the following abstract inverse problem or parameter identification problem

$$(1) \quad \mathbf{y} = \mathcal{G}(\mathbf{u}) + \boldsymbol{\eta}$$

aiming to recover unknown control $\mathbf{u} \in X$ from given observations $\mathbf{y} \in Y$, where $\boldsymbol{\eta}$ is observational noise. Typically, $\boldsymbol{\eta}$ is not explicitly known but only information on its distribution is available. We assume that $\boldsymbol{\eta} \sim \mathcal{N}(\mathbf{0}, \boldsymbol{\Gamma}^{-1})$, i.e. the observational noise is normally distributed with zero mean and given covariance matrix $\boldsymbol{\Gamma}^{-1} \in \mathbb{R}^{K \times K}$.

The EnKF can be derived within the inverse problem framework by rewriting (1) as a partially observed and artificial dynamical system based on state augmentation, e.g. cf. [3, 18]. The update formula for each ensemble member is computed by imposing first order necessary optimality conditions to solve a regularized minimization problem, which aims for a compromise between the background estimate of the dynamics model and additional information provided by data model. A similar technique is used to derive the update formula for constrained inverse problems [2, 17].

In order to understand how and why the EnKF works, a continuous-time limit [4, 5, 8, 22, 23] and a mean-field limit on the number of the ensemble members [7, 9, 12, 16] have been developed. Recent theoretical progress [16, 22] using these limits is the starting point of the current work. Specifically, it has been shown that, within these limits, the EnKF provides a solution to the inverse problem (1) by minimizing the least-squares functional

$$(2) \quad \Phi(\mathbf{u}, \mathbf{y}) := \frac{1}{2} \left\| \boldsymbol{\Gamma}^{\frac{1}{2}}(\mathbf{y} - \mathcal{G}(\mathbf{u})) \right\|_Y^2,$$

via a preconditioned gradient flow equation, where the preconditioner is given by the empirical covariance of the ensemble. Note that, contrary to the fully discrete and classical formulation of the EnKF, there is no regularization of the control \mathbf{u} in the minimization of (2). However, when the inverse problem is ill-posed, infimization of Φ is not a well-posed problem and some form of regularization may be required. This has been recognized in [8, 28] where modifications of the EnKF are proposed, leading to Tikhonov-Phillips-like regularizations of (2).

Another source of problems is given by the preconditioned gradient flow structure. In [16] a linear stability analysis of the moment equations revealed that the method has infinitely many non-hyperbolic Bogdanov-Takens equilibria [13] that lie on the set where the preconditioner collapse to zero. Not only are Bogdanov-Takens equilibria not asymptotically stable

they are structurally unstable and thus non robust and extremely sensitive to model perturbations. If the collapse happens too fast, convergence to the solution of the minimization of (2), cannot be reached anymore leading to convergence that depends on choosing a proper initial ensemble.

In this work we address these issues by introducing a modification of the continuous dynamics for the ensemble, in such a way the corresponding phase plane of the moment equations is characterized by a globally asymptotically stable equilibrium, the one minimizing the least-squares functional (2). The stabilization effect is obtained by artificially inflating the preconditioner of the gradient flow equation and by adding a suitable regularization term aiming to control the distance of each ensemble member to their mean. The usual properties of the classical ensemble Kalman filter, such as decay of the ensemble spread, are still satisfied by this stabilized version of the method. Its performance is investigated for a two-dimensional inverse problem. We show that the new method is able to converge to the solution faster and, more importantly, converges independently of the initial guess of the ensemble.

The rest of the paper is organized as follows. In Section 2 we review the ensemble Kalman filter formulation for inverse problems and the continuous formulations. In particular, the linear stability analysis of the moment equations performed in [16] is recalled. In Section 3 we discuss the stabilization of the dynamics and analyze the properties of the regularized method. In Section 4 we investigate the ability of the method to provide solution to an inverse problem based on a two-dimensional elliptic PDE. Finally, we summarize the results in Section 5.

2 Preliminaries on the Ensemble Kalman Filter for Inverse Problems

We briefly recall the original formulation of the Ensemble Kalman Filter (EnKF), cf. [10], which is based on a sequential update of an ensemble to estimate the solution of control-to-observable inverse problems. The derivation of the method is presented within optimization theory. Focusing on recent continuous limit formulations which have allowed theoretical analysis of the nature of the method, we review the one-dimensional linear stability analysis of the moment equations performed in [16].

2.1 Ensemble Kalman Filter

We consider a number J of ensembles (realizations of the control) combined in $\mathbf{U} = \{\mathbf{u}^j\}_{j=1}^J$. The EnKF is originally posed as a discrete iteration on \mathbf{U} , derived by solving a minimization problem that compromises between the background estimate of the given model and additional information provided by data or measurements. For more details, we refer e.g. to [18]. The iteration index is denoted by n and the collection of the ensembles by $\mathbf{u}^{j,n} \in \mathbb{R}^d$, $\forall j = 1, \dots, J$ and $n \geq 0$. The EnKF iterates each component of \mathbf{U}^n at iteration $n + 1$ as

$$(3) \quad \mathbf{u}^{j,n+1} = \mathbf{u}^{j,n} + \mathbf{C}_{\mathcal{G}}(\mathbf{U}^n) \left(\mathbf{D}_{\mathcal{G}}(\mathbf{U}^n) + \frac{1}{\Delta t} \mathbf{\Gamma}^{-1} \right)^{-1} (\mathbf{y} - \mathcal{G}(\mathbf{u}^{j,n}))$$

for each $j = 1, \dots, J$ where $\Delta t \in \mathbb{R}^+$ is a parameter. In general, each observation or measurement can be perturbed by additive noise [18]. We focus on the case where the measurement data $\mathbf{y} \in \mathbb{R}^K$ is unperturbed.

The update of the ensemble (3) requires the knowledge of the operators $\mathbf{C}_{\mathcal{G}}(\mathbf{U}^n)$ and $\mathbf{D}_{\mathcal{G}}(\mathbf{U}^n)$ which are the covariance matrices depending on the ensemble set \mathbf{U}^n at iteration n and on $\mathcal{G}(\mathbf{U}^n)$, i.e. the image of \mathbf{U}^n at iteration n . More precisely, we have

$$(4) \quad \begin{aligned} \mathbf{C}_{\mathcal{G}}(\mathbf{U}^n) &= \frac{1}{J} \sum_{k=1}^J (\mathbf{u}^{k,n} - \bar{\mathbf{u}}^n) \otimes (\mathcal{G}(\mathbf{u}^{k,n}) - \bar{\mathcal{G}}^n) \in \mathbb{R}^{d \times K} \\ \mathbf{D}_{\mathcal{G}}(\mathbf{U}^n) &= \frac{1}{J} \sum_{k=1}^J (\mathcal{G}(\mathbf{u}^{k,n}) - \bar{\mathcal{G}}^n) \otimes (\mathcal{G}(\mathbf{u}^{k,n}) - \bar{\mathcal{G}}^n) \in \mathbb{R}^{K \times K} \end{aligned}$$

where we define $\bar{\mathbf{u}}^n$ and $\bar{\mathcal{G}}^n$ as the mean of \mathbf{U}^n and $\mathcal{G}(\mathbf{U}^n)$, respectively:

$$\bar{\mathbf{u}}^n = \frac{1}{J} \sum_{j=1}^J \mathbf{u}^{j,n}, \quad \bar{\mathcal{G}}^n = \frac{1}{J} \sum_{j=1}^J \mathcal{G}(\mathbf{u}^{j,n}).$$

The EnKF satisfies the subspace property [18], i.e. the ensemble iterates stay in the subspace spanned by the initial ensemble. As consequence, the natural estimator for the solution of the inverse problem is provided by the mean of the ensemble.

2.2 Derivation of the Ensemble Kalman Filter from an Optimization Point-of-View.

The EnKF method (3) for the solution of the inverse problem (1) can be derived by using an optimization point-of-view. We introduce a new variable $\mathbf{w} = \mathcal{G}(\mathbf{u}) \in \mathbb{R}^K$ and reformulate (1) equivalently as

$$\begin{aligned} \mathbf{w} &= \mathcal{G}(\mathbf{u}) \\ \mathbf{y} &= \mathbf{w} + \boldsymbol{\eta}. \end{aligned}$$

The problem is then reinterpreted as filtering problem by considering a discrete-time dynamical system with state transitions and noisy observations:

$$\begin{aligned} \text{(dynamics model)} \quad & \begin{cases} \mathbf{u}^{n+1} = \mathbf{u}^n \\ \mathbf{w}^{n+1} = \mathcal{G}(\mathbf{u}^n) \end{cases} \\ \text{(data model)} \quad & \mathbf{y} = \mathbf{w}^{n+1} + \boldsymbol{\eta}. \end{aligned}$$

By defining $\mathbf{v} = [\mathbf{u}, \mathbf{w}]^T \in \mathbb{R}^{d+K}$ and $\Xi : \mathbf{v} \mapsto \Xi(\mathbf{v}) = [\mathbf{u}, \mathcal{G}(\mathbf{u})]^T \in \mathbb{R}^{d+K}$, the dynamical model can be written as

$$\mathbf{v}^{n+1} = \Xi(\mathbf{v}^n),$$

whereas the data model becomes

$$\mathbf{y} = \mathbf{H}\mathbf{v}^{n+1} + \boldsymbol{\eta},$$

where $\mathbf{H} = [\mathbf{0}_{K \times d}, \mathbf{I}_{K \times K}] \in \mathbb{R}^{K \times (d+K)}$ is an observation matrix. Let us denote by $\{\mathbf{v}^{j,n}\}_{j=1}^J$ a collection of J ensemble members, also called particles, at time n . The method proceeds as follows.

First, the state of all particles at time $n+1$ is predicted using the dynamical model to give $\{\hat{\mathbf{v}}^{j,n+1}\}_{j=1}^J$, i.e. $\hat{\mathbf{v}}^{j,n+1} = \Xi(\mathbf{v}^{j,n})$. The resulting empirical covariance $\mathbf{Cov} \in \mathbb{R}^{(d+K) \times (d+K)}$ of the uncertainties in the predictions is computed. Exploiting the definition of Ξ it is easy to check that

$$\mathbf{Cov} = \frac{1}{J} \sum_{k=1}^J (\hat{\mathbf{v}}^{k,n+1} - \bar{\mathbf{v}}^{n+1}) \otimes (\hat{\mathbf{v}}^{k,n+1} - \bar{\mathbf{v}}^{n+1}) = \begin{bmatrix} \mathbf{C} & \mathbf{C}_{\mathcal{G}} \\ \mathbf{C}_{\mathcal{G}}^T & \mathbf{D}_{\mathcal{G}} \end{bmatrix},$$

where $\mathbf{C}_{\mathcal{G}}$ and $\mathbf{D}_{\mathcal{G}}$ are as in (4), whereas

$$\mathbf{C} = \frac{1}{J} \sum_{k=1}^J (\mathbf{u}^{k,n} - \bar{\mathbf{u}}^n) \otimes (\mathbf{u}^{k,n} - \bar{\mathbf{u}}^n).$$

Then, the update $\mathbf{v}^{j,n+1}$ of each particle is determined by imposing first order necessary optimality condition of the following minimization problem

$$\mathbf{v}^{j,n+1} = \arg \min_{\mathbf{v}} \mathcal{J}^{j,n}(\mathbf{v}),$$

which is solved sequentially, and where $\mathcal{J}^{j,n}(\mathbf{v})$ is the objective function which encapsulates the model–data compromise:

$$(5) \quad \mathcal{J}^{j,n}(\mathbf{v}) = \frac{1}{2} \|\mathbf{y}^{n+1} - \mathbf{H}\mathbf{v}\|_{\Gamma^{-1}}^2 + \frac{1}{2} \|\mathbf{v} - \hat{\mathbf{v}}^{j,n+1}\|_{\mathbf{Cov}}^2.$$

Finally, the update (3) of $\mathbf{u}^{j,n+1}$, related to the unknown control state only, is obtained as $\mathbf{H}^\perp \mathbf{v}^{j,n+1}$, with $\mathbf{H}^\perp = [\mathbf{I}_{d \times d}, \mathbf{0}_{d \times K}] \in \mathbb{R}^{d \times (d+K)}$.

For further details and explicit computations we refer to e.g. [2].

This derivation of the ensemble Kalman filter from an optimization point-of-view leads into the introduction and motivation of the stabilized formulation of the continuous limit. In particular, we observe that the first term of the objective (5) corresponds to the least-squares functional Φ given by (2). Therefore, minimization of (5) can be seen as minimization of Φ subject to a regularization term involving the covariance of the ensemble.

Remark 1. *The derivation of the EnKF motivated through the optimization approach assumes that the empirical covariance \mathbf{Cov} is positive definite $\forall n \geq 0$. In general, it is not possible to guarantee that. In [2] and in [5, 26], this issue is overcome by a constant or time dependent shifting of \mathbf{Cov} .*

2.3 Continuous Limits of the Ensemble Kalman Filter

2.3.1 Continuous-time

As in [22], we compute the continuous-time limit equation of the update (3). We consider the parameter Δt as an artificial time step for the discrete iteration, i.e. $\Delta t \sim N_t^{-1}$ with N_t

being the maximum number of iterations and define $\mathbf{U}^n \approx \mathbf{U}(n\Delta t) = \{\mathbf{u}^j(n\Delta t)\}_{j=1}^J$ for $n \geq 0$. Computing the limit $\Delta t \rightarrow 0^+$ we obtain

$$(6) \quad \begin{aligned} \frac{d}{dt} \mathbf{u}^j &= \mathbf{C}_{\mathcal{G}}(\mathbf{U}) \Gamma(\mathbf{y} - \mathcal{G}(\mathbf{u}^j)), \quad j = 1, \dots, J \\ \mathbf{C}_{\mathcal{G}}(\mathbf{U}) &= \frac{1}{J} \sum_{k=1}^J (\mathbf{u}^k - \bar{\mathbf{u}}) \otimes (\mathcal{G}(\mathbf{u}^k) - \bar{\mathcal{G}}) \end{aligned}$$

with initial condition $\mathbf{U}(0) = \mathbf{U}^0$. Let us consider the case of \mathcal{G} linear, i.e. $\mathcal{G}(\mathbf{u}) = \mathbf{G}\mathbf{u}$, with $\mathbf{G} \in \mathbb{R}^{K \times d}$. Then (6) is a gradient descent equation and we can write $\mathbf{C}_{\mathcal{G}}(\mathbf{U}) = \frac{1}{J} \sum_{k=1}^J (\mathbf{u}^k - \bar{\mathbf{u}}) (\mathbf{u}^k - \bar{\mathbf{u}})^T \mathbf{G}^T$. Since the least-squares functional (2) yields

$$(7) \quad \nabla_{\mathbf{u}} \Phi(\mathbf{u}, \mathbf{y}) = -\mathbf{G}^T \Gamma(\mathbf{y} - \mathbf{G}\mathbf{u}),$$

equation (6) can be stated in terms of the gradient of Φ as

$$(8) \quad \begin{aligned} \frac{d}{dt} \mathbf{u}^j &= -\mathbf{C}(\mathbf{U}) \nabla_{\mathbf{u}} \Phi(\mathbf{u}^j, \mathbf{y}), \quad j = 1, \dots, J \\ \mathbf{C}(\mathbf{U}) &= \frac{1}{J} \sum_{k=1}^J (\mathbf{u}^k - \bar{\mathbf{u}}) \otimes (\mathbf{u}^k - \bar{\mathbf{u}}). \end{aligned}$$

Equation (8) describes a preconditioned gradient descent equation for each ensemble aiming to minimize Φ . $\mathbf{C}(\mathbf{U})$ is positive semi-definite and hence

$$(9) \quad \frac{d}{dt} \Phi(\mathbf{u}(t), \mathbf{y}) = \frac{d}{dt} \frac{1}{2} \left\| \Gamma^{\frac{1}{2}} (\mathbf{y} - \mathbf{G}\mathbf{u}) \right\|^2 \leq 0.$$

Although the forward operator is assumed to be linear, the gradient flow is nonlinear. For further details and properties of the gradient descent equation (8) we refer to [22]. In particular, the subspace property of the EnKF also holds for the continuous dynamics.

Note that, in the continuous-time limit a term originally present in the fully-discrete EnKF method (3) is lost, cf. (5). This is due to the scaling assumption of the measurement covariance by Δt which makes the term of order Δt^2 . This term is however not a Tikhonov regularization-type term but may act as regularization term. We will come back to this point in Section 3.2.

2.3.2 Mean-field

By definition, the EnKF method is a computational method and hence is calculated for a finite ensemble size. The behavior of the method in the limit of infinitely many ensembles can be studied via mean-field limit leading to a Vlasov-type kinetic equation for the compactly supported on \mathbb{R}^d probability density of \mathbf{u} at time t , denoted by

$$(10) \quad f = f(t, \mathbf{u}) : \mathbb{R}^+ \times \mathbb{R}^d \rightarrow \mathbb{R}^+.$$

First we show the limit equation for the case of a non-linear model and later specialize it to a linear model \mathbf{G} . We follow the classical formal derivation to formulate a mean-field

equation of a particle system, see [6, 14, 21, 27]. We introduce the first moments $\mathbf{m} \in \mathbb{R}^d$, $\mathbf{m}_{\mathcal{G}} \in \mathbb{R}^K$ and the second moments $\mathbf{E} \in \mathbb{R}^{d \times d}$, $\mathbf{E}_{\mathcal{G}} \in \mathbb{R}^{d \times K}$ of f at time t , respectively, as

$$(11) \quad \begin{aligned} \mathbf{m}(t) &= \int_{\mathbb{R}^d} \mathbf{u} f(t, \mathbf{u}) d\mathbf{u}, & \mathbf{E}(t) &= \int_{\mathbb{R}^d} \mathbf{u} \otimes \mathbf{u} f(t, \mathbf{u}) d\mathbf{u}, \\ \mathbf{m}_{\mathcal{G}}(t) &= \int_{\mathbb{R}^d} \mathcal{G}(\mathbf{u}) f(t, \mathbf{u}) d\mathbf{u}, & \mathbf{E}_{\mathcal{G}}(t) &= \int_{\mathbb{R}^d} \mathbf{u} \otimes \mathcal{G}(\mathbf{u}) f(t, \mathbf{u}) d\mathbf{u}. \end{aligned}$$

Since $\mathbf{u} \in \mathbb{R}^d$, the corresponding discrete measure on the ensemble set $\mathbf{U} = \{\mathbf{u}^j\}_{j=1}^J$ is given by the empirical measure

$$(12) \quad f(t, \mathbf{u}) = \frac{1}{J} \sum_{j=1}^J \delta(\mathbf{u}^j - \mathbf{u}).$$

Let us consider the interacting particle system (6). The empirical measure allows for a mean-field limit of $\mathbf{C}_{\mathcal{G}}$ as

$$(\mathbf{C}_{\mathcal{G}})_{\kappa, \ell} = \int_{\mathbb{R}^d} u_{\kappa} \mathcal{G}(u)_{\ell} f(t, \mathbf{u}) d\mathbf{u} - \int_{\mathbb{R}^d} u_{\kappa} f(t, \mathbf{u}) d\mathbf{u} \int_{\mathbb{R}^d} \mathcal{G}(u)_{\ell} f(t, \mathbf{u}) d\mathbf{u}, \quad \kappa, \ell = 1, \dots, d$$

and therefore $\mathbf{C}_{\mathcal{G}}$ can be written in terms of the moments (11) of f only as

$$(13) \quad \mathbf{C}_{\mathcal{G}}(f) = \mathbf{E}_{\mathcal{G}}(t) - \mathbf{m}(t) \otimes \mathbf{m}_{\mathcal{G}}(t) \geq 0.$$

We denote a sufficiently smooth test function by $\varphi(\mathbf{u}) \in C_0^1(\mathbb{R}^d)$ and compute

$$\begin{aligned} \frac{d}{dt} \langle f, \varphi \rangle &= \frac{d}{dt} \int_{\mathbb{R}^d} \frac{1}{J} \sum_{j=1}^J \delta(\mathbf{u} - \mathbf{u}^j) \varphi(\mathbf{u}) d\mathbf{u} = -\frac{1}{J} \sum_{j=1}^J \nabla_{\mathbf{u}} \varphi(\mathbf{u}^j) \cdot \mathbf{C}_{\mathcal{G}}(f) \Gamma(\mathbf{y} - \mathcal{G}(\mathbf{u}^j)) \\ &= - \int_{\mathbb{R}^d} \nabla_{\mathbf{u}} \varphi(\mathbf{u}) \cdot \mathbf{C}_{\mathcal{G}}(f) \Gamma(\mathbf{y} - \mathcal{G}(\mathbf{u})) f(t, \mathbf{u}) d\mathbf{u} \end{aligned}$$

which finally leads to the strong form of the mean-field kinetic equation corresponding to the continuous-time limit (6):

$$(14) \quad \partial_t f(t, \mathbf{u}) - \nabla_{\mathbf{u}} \cdot (\mathbf{C}_{\mathcal{G}}(f) \Gamma(\mathbf{y} - \mathcal{G}(\mathbf{u})) f(t, \mathbf{u})) = 0.$$

In case of a linear model $\mathcal{G}(\cdot) = \mathbf{G} \cdot$ the mean-field kinetic equation corresponding to the gradient descent equation (8) becomes

$$(15) \quad \partial_t f(t, \mathbf{u}) - \nabla_{\mathbf{u}} \cdot (\mathbf{C}(f) \nabla_{\mathbf{u}} \Phi(\mathbf{u}, \mathbf{y}) f(t, \mathbf{u})) = 0.$$

where, similarly to $\mathbf{C}_{\mathcal{G}}(f)$, the operator $\mathbf{C}(f)$ can be also defined in terms of moments of the empirical measure (12) as

$$(16) \quad \mathbf{C}(f) = \mathbf{E}(t) - \mathbf{m}(t) \otimes \mathbf{m}(t) \geq 0.$$

We observe that (15) is a nonlinear transport equation arising from non-linear gradient flow interactions and the counterpart of (9) holds at the kinetic level. Defining

$$\mathcal{L}(f, \mathbf{y}) = \int_{\mathbb{R}^d} \Phi(\mathbf{u}, \mathbf{y}) f(t, \mathbf{u}) d\mathbf{u}$$

we compute

$$\frac{d}{dt}\mathcal{L}(f, \mathbf{y}) = \int_{\mathbb{R}^d} \Phi(\mathbf{u}, \mathbf{y}) \partial_t f(t, \mathbf{u}) d\mathbf{u} = - \int_{\mathbb{R}^d} (\nabla_{\mathbf{u}} \Phi(\mathbf{u}, \mathbf{y}))^T \mathbf{C}(f) \nabla_{\mathbf{u}} \Phi(\mathbf{u}, \mathbf{y}) d\mathbf{u} \leq 0$$

since $\mathbf{C}(f)$ is positive semi-definite. In particular, $\mathcal{L}(f, \mathbf{y})$ is decreasing unless f is a Dirac distribution. This consideration reveals again that a solution of $\min_{\mathbf{u} \in \mathbb{R}^d} \Phi(\mathbf{u}, \mathbf{y})$ provides a steady solution of the continuous–limit formulation, but the converse is not necessarily true. In particular, the velocity of convergence to the *correct* Dirac distribution may be highly influenced by the initial condition, i.e. by the distribution of the initial ensemble.

For the rigorous mean–field derivation and analysis of the EnKF we refer to [7, 9].

2.4 Stability of the Moment Equations

In [16], the linear stability analysis of the moment equations resulting from (15) has been investigated for one–dimensional controls. We recall that the expected value of the ensemble is selected as estimator for the solution, due to the subspace property satisfied by the EnKF. For this reason the analysis of moments is of crucial importance. Here, we briefly review this analysis, and therefore we restrict the attention to the case $d = K = 1$. From now on, we avoid using bold font to emphasize when the involved quantities are one–dimensional.

The dynamical system for the first and second moment is computed from (15). Using the linearity of the model we obtain

$$(17) \quad \begin{aligned} \frac{d}{dt} m(t) &= -C(m, E) G^T \Gamma (y - Gm) \\ \frac{d}{dt} E(t) &= 2C(m, E) G^T \Gamma (ym - GE), \end{aligned}$$

where we observe that $C(m, E)$ corresponds to the variance, in fact

$$\int_{\mathbb{R}} (u - m(t))^2 f(t, u) du = E(t) - m(t)^2.$$

System (17) is closed by the second moment equation.

We analyze steady–states and their stability with $G = \Gamma = 1$. Nullclines of (17) are

$$\begin{aligned} m &= y, E = m^2 \\ E &= ym, E = m^2. \end{aligned}$$

Equilibrium points arise by intersection of the nullclines and are given by

$$(18) \quad F_k = (k, k^2), \quad k \in \mathbb{R},$$

i.e. all equilibria are points on the set $E = m^2$ for which $C = 0$. We note that they lie on the boundary of the admissible region $C \geq 0$. This means that all Dirac delta distributions are steady–states of the mean–field equation, as shown for cases of arbitrary dimension at the end of Section 2.3. As consequence we have a set of infinitely many steady–states. The one minimizing the least square functional Φ is $\delta(u - y)$, corresponding to $F_y = (y, y^2)$. Studying the linear stability of the equilibrium points it is simple to show that all the F_k 's have

double-zero eigenvalues and are non-hyperbolic Bogdanov–Takens–type equilibria. This has several undesirable consequences: Bogdanov–Takens equilibria are not asymptotically stable, in fact their linearization is unstable. More importantly, they are non-hyperbolic and thus structurally unstable, i.e. susceptible to qualitative changes under arbitrary small perturbations of the underlying model.

3 Stabilization of the Dynamics

We will introduce a modified formulation of the continuous limit of the ensemble Kalman filter such that the desired equilibrium $F_y = (y, y^2)$ is a globally asymptotically stable equilibrium of the system of moment equations. We are only interested in the equilibrium F_y since the others are irrelevant for the optimization. The modification we propose is inspired by the idea to restore the regularization effect of the classical EnKF which gets lost in the continuous limit.

We propose to consider the following general discrete dynamics for each ensemble member $j = 1, \dots, J$:

$$\begin{aligned}
\frac{d}{dt} \mathbf{u}^j &= \tilde{\mathbf{C}}_{\mathcal{G}}(\mathbf{U}) \Gamma(\mathbf{y} - \mathcal{G}(\mathbf{u}^j)) + R(\mathbf{U}), \\
R(\mathbf{U}) &= \beta \tilde{\mathbf{C}}(\mathbf{U})(\mathbf{u}^j - \bar{\mathbf{u}}), \\
\tilde{\mathbf{C}}_{\mathcal{G}}(\mathbf{U}) &= \frac{1}{J} \sum_{k=1}^J (\mathbf{u}^k - \kappa \bar{\mathbf{u}}) \otimes (\mathcal{G}(\mathbf{u}^k) - \kappa \bar{\mathcal{G}}), \\
\tilde{\mathbf{C}}(\mathbf{U}) &= \frac{1}{J} \sum_{k=1}^J (\mathbf{u}^k - \kappa \bar{\mathbf{u}}) \otimes (\mathbf{u}^k - \kappa \bar{\mathbf{u}}),
\end{aligned}
\tag{19}$$

with $\kappa, \beta \in \mathbb{R}$. The choices $\kappa = 1$ and $\beta = 0$ yield continuous–time limit (6) for the original ensemble Kalman filter.

Remark 2. *We do not claim uniqueness for the modeling choice of the term $R(\mathbf{U})$. For instance $R(\mathbf{U}) = \beta \mathbf{u}^j$ would correspond to a Tikhonov–type regularization studied in [8]. Alternatively, [16] modified the discrete dynamics with additive white Gaussian noise. This approach leads to a Fokker–Planck–type equation, where Dirac delta distributions are no longer steady states and the desired equilibrium, F_y , depends on the nonzero variance σ of the noise and becomes $(y, y^2 \pm \sqrt{2\sigma^2})$.*

3.1 Linear stability analysis of moment equations

The analysis of stability of the new dynamics (19) is performed in the case of a linear model $\mathcal{G}(\cdot) = \mathbf{G}\cdot$. Then, (19) becomes

$$\begin{aligned}
\frac{d}{dt} \mathbf{u}^j &= -\tilde{\mathbf{C}}(\mathbf{U}) \nabla_{\mathbf{u}} \Phi(\mathbf{u}^j, \mathbf{y}) + R(\mathbf{U}), \\
R(\mathbf{U}) &= \beta \tilde{\mathbf{C}}(\mathbf{U})(\mathbf{u}^j - \bar{\mathbf{u}}), \\
\tilde{\mathbf{C}}(\mathbf{U}) &= \frac{1}{J} \sum_{k=1}^J (\mathbf{u}^k - \kappa \bar{\mathbf{u}}) \otimes (\mathbf{u}^k - \kappa \bar{\mathbf{u}}),
\end{aligned}
\tag{20}$$

with Φ being the least-squares functional (2).

The dynamical system (20) allows for a mean-field interpretation

$$(21) \quad \partial_t f(t, \mathbf{u}) - \nabla_{\mathbf{u}} \cdot \left(\tilde{\mathbf{C}}(f) (\nabla_{\mathbf{u}} \Phi(\mathbf{u}, \mathbf{y}) - \beta(\mathbf{u} - \mathbf{m})) f(t, \mathbf{u}) \right) = 0,$$

where

$$\tilde{\mathbf{C}}(f) = \mathbf{E} - \alpha \mathbf{m} \otimes \mathbf{m}$$

with $\alpha = \kappa(2 - \kappa)$. Note that $\tilde{\mathbf{C}}(f) \equiv \mathbf{E} - \mathbf{m} \otimes \mathbf{m} = \mathbf{C}(f) \geq 0$, if $\alpha = 1$, see (16).

The stability of moments is again studied in the simplest setting of a one-dimensional problem, i.e. $d = K = 1$. From (21) we compute

$$(22) \quad \begin{aligned} \frac{d}{dt} m &= \tilde{\mathbf{C}}(m, E) G^T \Gamma (y - Gm) \\ \frac{d}{dt} E &= 2\tilde{\mathbf{C}}(m, E) \left(G^T \Gamma (ym - GE) + \beta C(m, E) \right) \\ \tilde{\mathbf{C}}(m, E) &= (E - \alpha m^2) \\ C(m, E) &= (E - m^2), \end{aligned}$$

where we again avoid the use of bold fonts to highlight the one-dimensional quantities. Initial conditions $(m(0), E(0)) \in \mathbb{R} \times \mathbb{R}^+$ of (22) need to satisfy $E(0) > m(0)^2$ and we say that a solution is admissible or belongs to the feasible domain if $t \in \mathbb{R}^+ \mapsto (m(t), E(t)) \in \mathbb{R} \times \mathbb{R}^+$ satisfies $E(t) \geq m(t)^2$.

Steady states are obtained as intersection of the nullclines of the system. We use $G = \Gamma = 1$ and get the following equilibrium points (m, E) :

$$(23) \quad F_y = (y, y^2), \quad F_{k, \alpha} = (k, \alpha k^2), \quad k \in \mathbb{R}.$$

Here, α plays the role of a bifurcation parameter. In fact, for $\alpha \rightarrow 1$ we recover the same equilibria as in the classical ensemble Kalman filter, cf. (18). Therefore, compared to the classical continuous-time formulation of the ensemble Kalman filter, the new ensemble update (20) still has infinitely many equilibria on the set $E = \alpha m^2$, but, in addition, has F_y as an isolated fixed point of the dynamics.

The Hartman–Grobman Theorem states that non-linear dynamical systems are locally topologically conjugate to their linearized formulations near hyperbolic fixed point. Thus, if F_y is hyperbolic and asymptotically stable, the local phase portrait of the non-linear system (22) is equivalent to that of its linearization $[\dot{m}, \dot{E}]^T = \mathbf{J}(m, E)[m, E]^T$, where $\mathbf{J}(m, E)$ is the Jacobian. The eigenvalues of the equilibrium point F_y are

$$(24) \quad \lambda_1^{F_y} = y^2(\alpha - 1), \quad \lambda_2^{F_y} = -2y^2(\beta - 1)(\alpha - 1),$$

and the eigenvalues of the equilibria $F_{k, \alpha}$ are

$$\lambda_1^{F_{k, \alpha}} = 0, \quad \lambda_2^{F_{k, \alpha}} = -2k(y - k\beta)(\alpha - 1), \quad \forall k \in \mathbb{R}.$$

Thus F_y is an asymptotically stable equilibrium if $\alpha < 1$ and $\beta < 1$.

We notice that $\alpha < 1$ automatically implies that, except for $k = 0$, all the other equilibria $F_{k, \alpha}$ are not feasible, i.e. cannot be obtained via mean-field, since then $C(m, E) < 0$. In addition, $F_{0, \alpha}$ is still a Bogdanov–Takens–type equilibrium.

The above discussion is formally summarized in the following Proposition:

Proposition 3.1. *Let $(m(0), E(0)) = (m_0, E_0)$ be an admissible initial condition of (22). Then, the dynamical system has two feasible equilibrium points, $F_y = (y, y^2)$ and $F_{0,\alpha} = (0, 0)$, $\forall \alpha \in \mathbb{R}$. In particular, $F_{0,\alpha}$ is a non-hyperbolic Bogdanov–Takens–type equilibrium, and F_y is an asymptotically stable equilibrium, namely $\exists \delta > 0$ such that if $\|(m_0, E_0) - F_y\| < \delta$ then $\lim_{t \rightarrow \infty} (m(t), E(t)) = F_y$, provided $\alpha < 1$ and $\beta < 1$.*

To prove global asymptotic stability for F_y we note that the relevant subset of the phase space in \mathbb{R}^2 is bounded by $m = 0$, $E = 0$ and $E = m^2$. It is easy to see that the vector field generated by (22) for $\alpha < 1$ is always pointing inwards. In addition, for large enough E and $\beta < 1$ solutions do not escape to infinity. Since the only equilibria in this region are on the boundary and since F_y is the only locally stable equilibrium, hence by the Poincaré–Bendixson Theorem we have the following Proposition:

Proposition 3.2. *The point $F_y = (y, y^2)$ is a globally asymptotically stable equilibrium of the dynamical system (22), namely $\lim_{t \rightarrow \infty} (m(t), E(t)) = F_y$ for any admissible initial condition $(m(0), E(0))$, provided $\alpha < 1$ and $\beta < 1$.*

We notice that F_y is also a point of the phase space where $C \equiv 0$, as it happens for the classical EnKF formulation. Below, we compare the decay of the variance $C(t) = E - m^2$ at equilibrium between the continuous–time limit of the classical EnKF formulation and the stabilized dynamics (20).

From the classical EnKF dynamics (8) we compute

$$\frac{d}{dt}C = \frac{d}{dt}E - 2m \frac{d}{dt}m = -2C^2$$

and thus C is decreasing in time with rate $\mathcal{O}(t^{-1})$. In fact, the solution is

$$C(t) = \frac{C(0)}{1 + 2C(0)t}.$$

Instead, in the stabilized version of the EnKF (20) we have

$$\frac{d}{dt}C = \frac{d}{dt}E - 2m \frac{d}{dt}m = -2(1 - \beta)\tilde{C}C \leq -2(1 - \beta)C^2$$

provided $\alpha < 1$ so that $0 \leq C < \tilde{C}$. Applying Gronwall inequality we obtain

$$C(t) \leq \frac{C(0)}{1 + 2(1 - \beta)C(0)t}$$

which implies a rate of decay $\mathcal{O}((1 - \beta)t^{-1})$ at least. In particular, we observe that the decay is faster for $\beta < 0$. We conclude that, while α plays the role of a bifurcation parameter leading to a change of the equilibria in the phase space, β plays the role of a regularization parameter speeding–up the convergence to the equilibrium F_y .

Remark 3. *We stress the fact that neither of the regularization approaches cited in Remark 2 has the property of stabilizing the moment dynamics by preserving the equilibrium F_y , and turning it into a globally asymptotically stable equilibrium.*

3.2 Analysis of the ensemble dynamics

It is possible to provide a gradient flow interpretation also for the stabilized dynamics (20). In fact, we observe that each ensemble is solving a preconditioned gradient descent equation of the type

$$\begin{aligned} \frac{d}{dt} \mathbf{u}^j &= -\tilde{\mathbf{C}}(\mathbf{U}) \nabla_{\mathbf{u}} \Psi(\mathbf{u}^j, \mathbf{y}, \mathbf{u}^{-j}) \\ \Psi(\mathbf{u}^j, \mathbf{y}, \mathbf{u}^{-j}) &= \Phi(\mathbf{u}^j, \mathbf{y}) + \frac{J\beta}{2(J-1)} \|\mathbf{u}^j - \bar{\mathbf{u}}\|^2, \end{aligned}$$

where we denote $\mathbf{u}^{-j} = \{\mathbf{u}^k\}_{\substack{k=1 \\ k \neq j}}^J$. Within this formulation we see that our modified dynamics again adds a regularization term. Existence and uniqueness of solutions to (20) is straightforward since the right-hand side is locally Lipschitz in \mathbf{u}^j , thus local existence of a solution in the space $\mathcal{C}([0, T])$ holds for some $T > 0$. We need to prove global existence, namely that the solution does not blow up in finite time, and this is guaranteed by Proposition 3.3 below.

We define for each $j = 1, \dots, J$

$$(25) \quad \mathbf{e}^j(t) = \mathbf{u}^j(t) - \bar{\mathbf{u}}(t),$$

$$(26) \quad \mathbf{r}^j(t) = \mathbf{u}^j(t) - \mathbf{u}^*$$

the ensemble spread and the residual to a value \mathbf{u}^* , respectively. Proposition 3.3 gives sufficient conditions for the existence of a monotonic decay for the ensemble spread.

Proposition 3.3. *Let $\mathbf{u}^j(0) \in \mathbb{R}^d$, $j = 1, \dots, J$, be an admissible initial condition of the dynamical system (20). The quantity $\|\mathbf{e}^j(t)\|^2$ is decreasing in time, i.e. $\|\mathbf{e}^j(t)\|^2 \leq \|\mathbf{e}^j(0)\|^2$, for each $j = 1, \dots, J$ and $t \geq 0$, provided that $\alpha < 1$ and $\beta < 0$. In particular, if $\mathbf{\Gamma}$ is positive definite then $\lim_{t \rightarrow \infty} \|\mathbf{e}^j(t)\|^2 = 0$.*

Proof. To prove the statement, it is sufficient to study the behavior of the covariance operator \mathbf{C} in time. Let us denote $\mathbf{I}_d \in \mathbb{R}^{d \times d}$ the identity matrix. The hypothesis $\alpha < 1$ implies $\tilde{\mathbf{C}}$ positive definite for all $t \geq 0$, and in particular $\mathbf{C} < \tilde{\mathbf{C}}$. Using $\beta < 0$ and the entry-wise matrix norm, we compute

$$\frac{d}{dt} \|\mathbf{C}\| < -2\|\langle \mathbf{C}, \mathbf{C} \rangle_{\mathbf{P}_\beta}\| \leq 0$$

where $\mathbf{P}_\beta = \mathbf{G}^T \mathbf{\Gamma} \mathbf{G} - \beta \mathbf{I}_d$. The last inequality is strict whenever $\mathbf{\Gamma}$ is positive definite. In particular we have the following bound

$$\mathbf{C}(t) = \left(2\mathbf{P}_\beta t + \mathbf{C}(0)^{-1} \right)^{-1},$$

and the velocity of decay is determined by the minimum eigenvalue of \mathbf{P}_β . \square

The previous result establishes sufficient conditions for the ensemble collapse to the mean $\bar{\mathbf{u}}$ in the long time behavior, and consequently each ensemble member solves at equilibrium the same minimization problem that $\bar{\mathbf{u}}$ is solving. With this consideration we state and prove the following result on the convergence of the residual in the control space.

Proposition 3.4. *Let $\mathbf{u}^j(0) \in \mathbb{R}^d$, $j = 1, \dots, J$, be an admissible initial condition of the dynamical system (20). Assume that Γ is positive definite and let \mathbf{u}^* be a KKT point of the minimization problem $\min_{\mathbf{u} \in \mathbb{R}^d} \Phi(\mathbf{u}, \mathbf{y})$. Then $\lim_{t \rightarrow \infty} \|\mathbf{r}^j(t)\|^2 = 0$, for each $j = 1, \dots, J$, provided that $\alpha < 1$ and $\beta < 0$.*

Proof. By assumption Γ is positive definite and thus we have a unique global minimizer \mathbf{u}^* of the minimization problem $\min_{\mathbf{u} \in \mathbb{R}^d} \Phi(\mathbf{u}, \mathbf{y})$, for a given $\mathbf{y} \in \mathbb{R}^K$. Moreover, for Proposition (3.3) it is sufficient to show that $\|\bar{\mathbf{u}} - \mathbf{u}^*\| \rightarrow 0$ as $t \rightarrow \infty$. The evolution equation of the ensemble mean is given by

$$\frac{d}{dt} \bar{\mathbf{u}} = -\tilde{\mathbf{C}} \nabla_{\mathbf{u}} \Phi(\bar{\mathbf{u}}, \mathbf{y}).$$

Then, since $\tilde{\mathbf{C}}$ is positive definite, at equilibrium the ensemble mean solves the equation $\nabla_{\mathbf{u}} \Phi(\bar{\mathbf{u}}, \mathbf{y}) = 0$. \square

Remark 4. *Contrary to the analysis in Section 3.1, where the global asymptotic stability of the dynamical system (22) is guaranteed by choosing $\beta < 1$, we observe that Proposition 3.3 and Proposition 3.4 assume $\beta < 0$. However, we stress the fact that this is a sufficient condition to show collapse of the ensemble and convergence to the residual. In order to strengthen this condition, and consider also values of $\beta \in [0, 1)$, one would need to ensure that the operator \mathbf{P}_β is positive (semi)-definite.*

4 Numerical simulations

4.1 Simulation of the moment dynamics

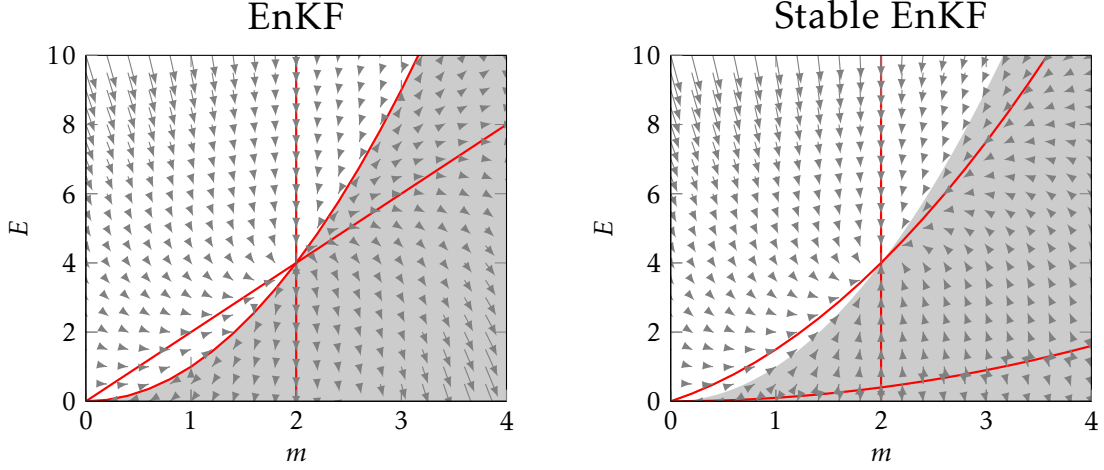
We recall that the stabilization of the continuous-time limit of the ensemble Kalman filter is motivated by a linear stability analysis of the moment equations, in the simplest case of a one-dimensional control. For this reason, we aim to compare the moment dynamics provided by the ensemble Kalman filter (6) and by the present stabilization of the method (19).

All simulations run with the same parameters used for the stability analysis in Section 3.1, namely we consider $G = \Gamma = 1$. The stabilizing parameters are $\alpha = 0.1$ and $\beta = -1$. Moreover, we set $y = 2$ so that the target equilibrium is $F_y = (2, 4)$.

In Figure 1 we show the phase portraits with the velocity field of the moment equations. The red lines are nullclines, and the gray-shaded area represents the unfeasible region where $E < m^2$. We observe that the stabilized version of the EnKF proposed in this work preserves the target equilibrium F_y . In the classical EnKF, Figure 1a, the nullcline on the border of the feasible region is a set of equilibrium points. The stabilization moves these equilibria on the red nullcline in the unfeasible region, see Figure 1b.

To provide additional numerical insight, we study the effect of the stabilization on the moment equations by looking at the time behavior of the covariance $\mathbf{C}(t) = E - m^2$ for two different initial conditions in both systems, the classical EnKF and the stabilized EnKF.

The initial conditions of the first moments are $m(0) = 1$ and $m(0) = 3$. The initial energy $E(0)$ is chosen such that $(m(0), E(0))$ is in the feasible region $\mathbf{C}(0) \geq 0$. The systems of moments are numerically solved with an explicit fourth-order Runge-Kutta method. In Figure 2, we observe that both, the stabilized EnKF and the classical EnKF show a variance decay to zero, i.e. collapse to a Dirac delta at mean-field level. However, noting the logarithmic scale in Figure 2 we see that the stable method decays to the equilibrium state much faster.



(a) The classical ensemble Kalman filter (17). (b) The stabilized ensemble Kalman filter (22).

Figure 1: Phase planes of the moment systems. Red lines are nullclines, the gray-shaded area represents the unfeasible region.

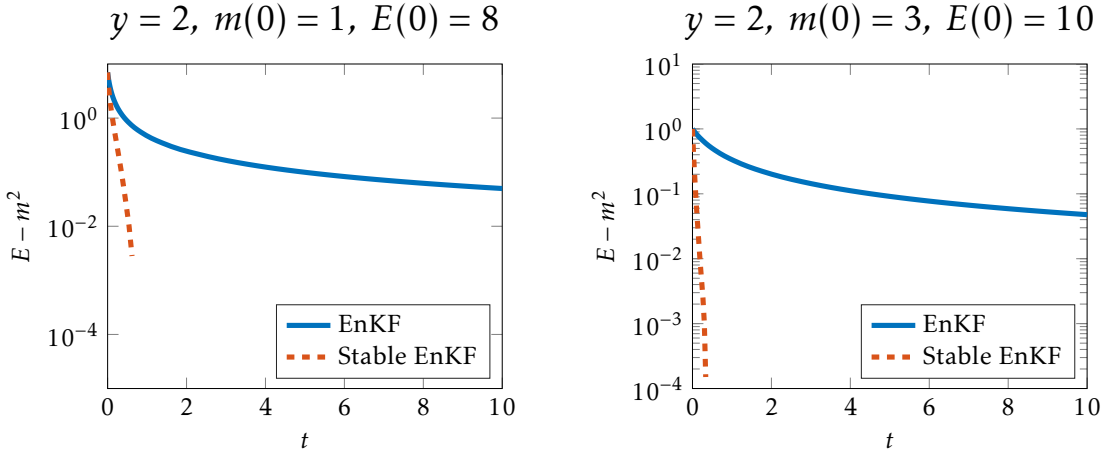


Figure 2: Variance evolution computed by solving the moment systems for the classical ensemble Kalman filter (17), and the stabilized ensemble Kalman filter (22), for two different sets of initial conditions.

4.2 A two-dimensional inverse problem

We consider the inverse problem of finding the hydraulic conductivity function of a non-linear elliptic equation in two spatial dimension assuming that noisy observation of the solution to the problem are available.

The problem is described by the following PDE modeling groundwater flow in a two-

dimensional confined aquifer:

$$(27) \quad \begin{aligned} -\nabla \cdot (e^{\log K} \nabla p) &= f \quad \text{in } \Omega = (-1, 1)^2 \\ p &= 0 \quad \text{on } \partial\Omega. \end{aligned}$$

Here, K is the hydraulic conductivity, f is the force function and the flow is described in terms of the piezometric head p . This problem has been intensively used in the literature on the ensemble Kalman filter to study performance of the method. E.g. see [8, 18, 22].

We aim to find the log conductivity $u = \log K$ from 400 observations of the solution p on a uniform grid in Ω . We choose $f = 100$. The mapping from u to these observations is now non-linear, and thus we need to employ the ensemble dynamics for the non-linear model (19).

Noise is assumed to be Gaussian distributed with covariance $\Gamma^{-1} = \gamma^2 \mathbf{I}$, with $\gamma = 4$. The prior is also Gaussian distributed with covariance $(-\Delta)^{-2}$, whose discretization is again computed by using homogeneous Dirichlet boundary conditions. We use a \mathbb{P}^1 FEM approximation. The ensemble size is chosen as $J = 100$. The ensemble dynamics (19) are numerically solved by explicit Euler discretization with fixed and, to avoid stability issues, small time step $\Delta t = 10^{-3}$. Final time for the simulations is $T = 1$.

In order to avoid over-fitting of the method, we employ the discrepancy principle as stopping criterion. Thus, we check and stop the simulation when the condition $\vartheta \leq \|\boldsymbol{\eta}\|^2$ is satisfied, where $\boldsymbol{\eta}$ is the measurement noise and

$$(28) \quad \vartheta = \frac{1}{J} \sum_{j=1}^J \|\mathcal{G}(\mathbf{u}^j) - \mathbf{p} - \boldsymbol{\eta}\|^2$$

is the misfit which allows to measure the quality of the solution at each iteration. Moreover, \mathbf{u}^j and \mathbf{p} are vectors containing the discrete values of the control for the j -th ensemble member and of the true observations, respectively. In this example \mathcal{G} is the \mathbb{P}^1 FEM discretization of the continuous operator defining the elliptic PDE (27).

The initial ensemble is drawn from a Gaussian distribution with given covariance matrix $\delta(-\Delta)^{-2}$, and we consider $\delta = 1$ and $\delta = 10^{-2}$. We compare results obtained with the continuous-time limit of the classical EnKF, i.e. when $\alpha = 1$ and $\beta = 0$, and with the stabilized method, using $\alpha = 0.9$ and $\beta = -1$.

In Figure 3 we show the time behavior of the misfit (28) (top row), of the residual (26) (middle row) and of the spread to the mean (25) (bottom row) provided by the two methods. The results in the left panel are obtained with $\delta = 1$, so that the initial ensemble is sampled from the same prior distribution of the exact control. The results in the right panel are computed with $\delta = 10^{-2}$ which mimics the situation where the initial covariance is $\mathbf{C}(0) = \mathbf{0}$, and hence close to the border of the feasible region. We observe that, if the distribution of the initial ensemble is properly chosen, i.e. when $\delta = 1$, the two methods meet the discrepancy principle, and the misfit, the residual and the ensemble spread decrease in time. The stabilized method allows to save about the 25% of the computational cost.

The difference between the two methods can be appreciated when the initial guess of the ensemble is not properly chosen, i.e. when $\delta = 10^{-2}$. This is relevant in applications, where the distribution of the unknown control is not known, therefore the ensemble cannot be suitably initialized leading to a possible change in the length of the transient. In fact, we

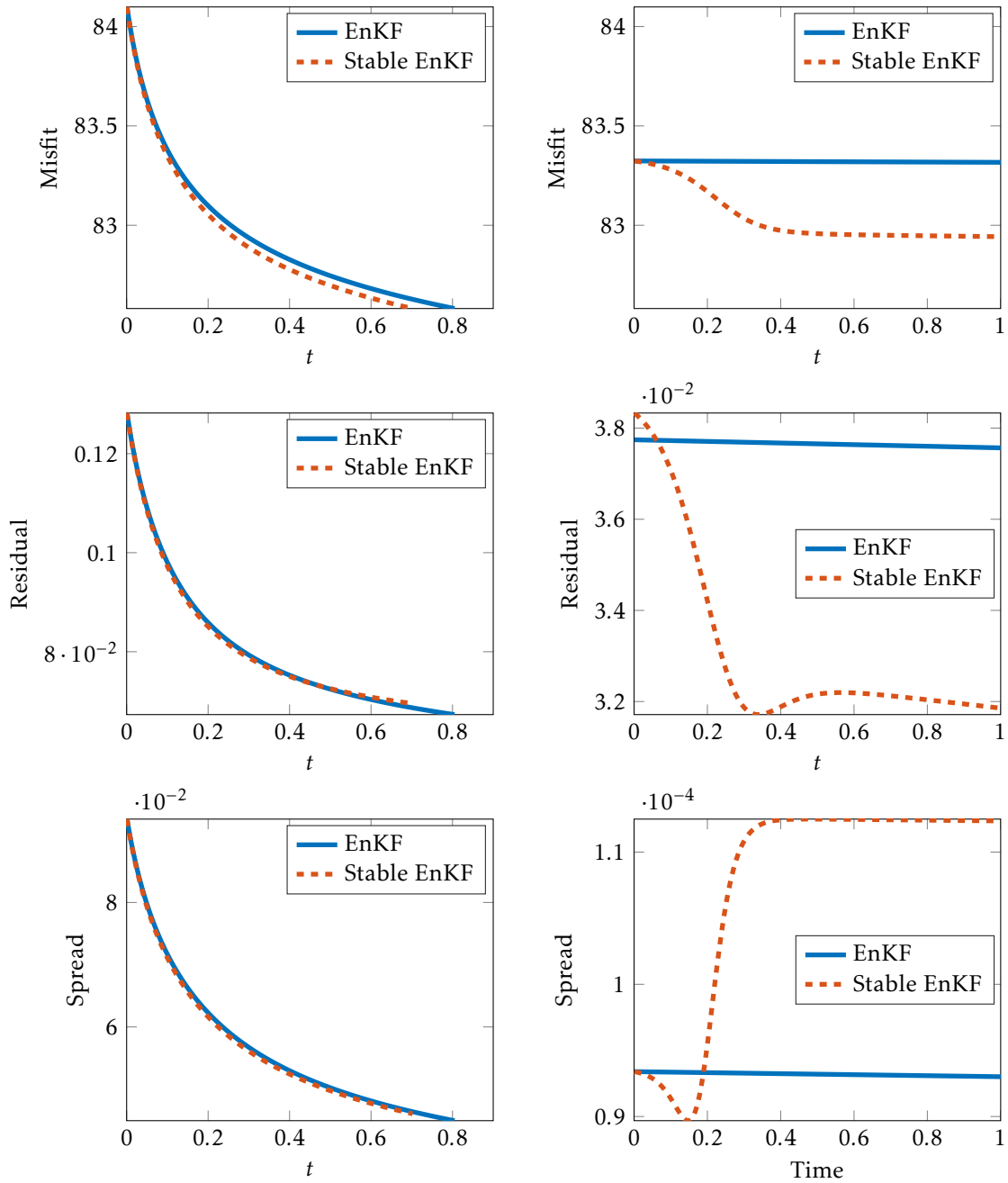


Figure 3: Misfit (28), residual (26) and spread (25) behavior in time for the inverse problem of determining the log conductivity $u = \log K$ for (27) using the classical ensemble Kalman filter (EnKF) (6) and the stabilized ensemble Kalman filter (Stable EnKF) (19). Left column: both methods converge for well chosen initial covariance ($\delta = 1$); right column: only the stabilized EnKF converges for a bad initial covariance ($\delta = 10^{-2}$).

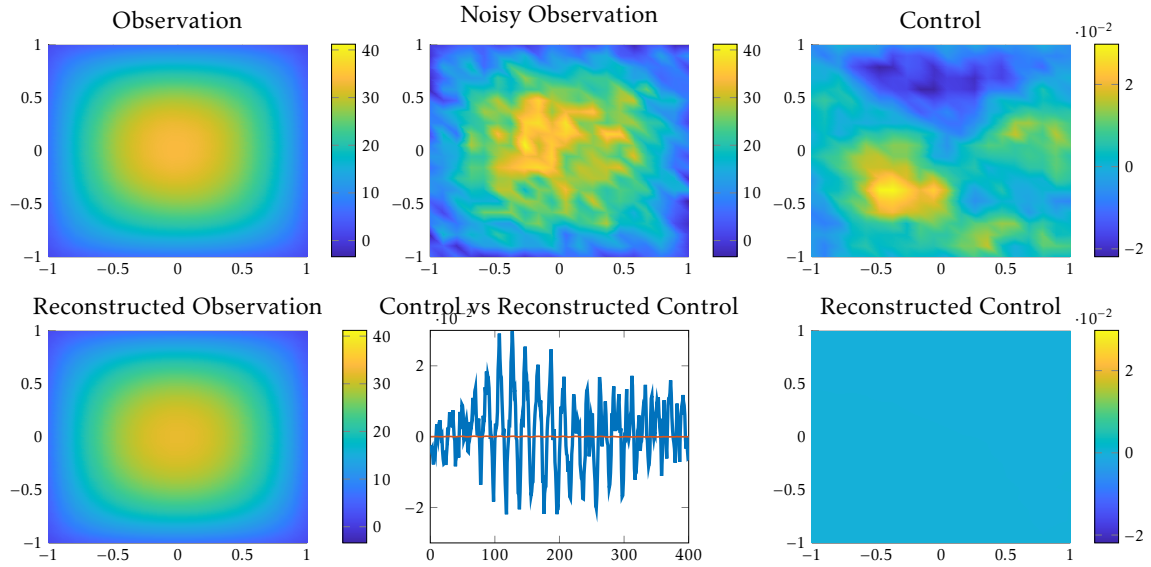


Figure 4: Inverse problem of determining the log conductivity $u = \log K$ for the two-dimensional groundwater equation (27) on a 20×20 grid, and solved by the continuous-time limit of the classical ensemble Kalman filter (6). From top right: discrete observations of the true solution p ; true observations perturbed by Gaussian noise; discrete true log conductivity u ; solution computed with the identified unknown; one-dimensional plot of the discrete true and reconstructed log conductivity; discrete reconstructed log conductivity.

observe that the stabilized version of the method provides a fast transient of the misfit, of the residual and of the ensemble spread in contrast to the classical EnKF which does not seem to converge.

This effect can be also observed by comparing the results in Figure 4, referred to the classical ensemble Kalman filter, and in Figure 5, for the stabilized version of the method. We consider the case $\delta = 10^{-2}$ only. The top-row panels of both figures are the same. They show, from left to right, the true solution p of (27) evaluated on a 20×20 uniform grid, the perturbed solution by additive Gaussian noise, and the a-priori artificially assigned true log conductivity u , i.e. the control in this example, which provides the solution p and we aim to identify. The bottom-row panels, instead, show the solution obtained with the reconstructed log conductivity, and the identified control itself using both a one-dimensional and a two-dimensional visualization. In these figures we appreciate the importance of the distribution of the initial ensemble in order to ensure that the classical method, i.e. when covariance inflation and regularization terms are not considered, is able to provide a good identification of the unknown control.

5 Conclusions

In this paper we have focused on the continuous limit formulations of the ensemble Kalman filter, recently introduced in [16, 22] to solve constrained inverse problems. We

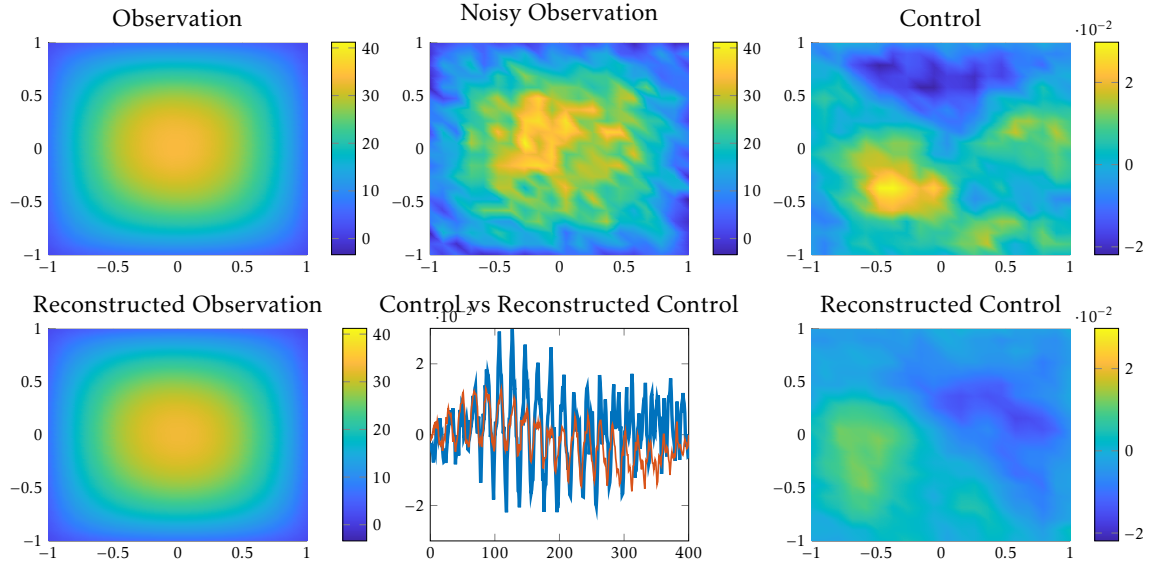


Figure 5: Inverse problem of determining the log conductivity $u = \log K$ for the two-dimensional groundwater equation (27) on a 20×20 grid, and solved by the stabilized ensemble Kalman filter method (19) with $\alpha = 0.9$ and $\beta = -1$. From top right: discrete observations of the true solution p ; true observations perturbed by Gaussian noise; discrete true log conductivity u ; solution computed with the identified unknown; one-dimensional plot of the discrete true and reconstructed log conductivity; discrete reconstructed log conductivity

have observed that these formulations provide a structurally unstable system of moment equations characterized by infinitely many equilibrium solutions, lying on the boundary of the feasible region and being unstable non-hyperbolic Bogdanov-Takens equilibria. We modify the ensemble dynamics by inflating the covariance operator and by adding a suitable regularization term leading to a system of moment equations which has a globally asymptotically stable equilibrium. The latter minimizes the least square functional. Properties of the ensemble dynamics have been also studied. The numerical results illustrate that the stabilized method is able to provide fast convergence to the solution, independently of the choice of the distribution for the initial ensemble.

Acknowledgments

This research is funded by the Deutsche Forschungsgemeinschaft (DFG, German Research Foundation) under Germany's Excellence Strategy – EXC-2023 Internet of Production – 390621612 and supported also by DFG HE5386/15. This work has been initiated during the workshop “Stochastic dynamics for complex networks and systems” hosted at the University of Mannheim in 2019. The workshop was financially supported by the DAAD exchange project PPP USA 2019 (project-id 57444394).

References

- [1] S. I. Aanonsen, G. Naevdal, D. S. Oliver, A. C. Reynolds, and B. Valles. The ensemble Kalman filter in reservoir engineering—a review. *SPE J.*, 14(3):393–412, 2009.
- [2] D. J. Albers, P.-A. Blancquart, M. E. Levine, E. E. Seylabi, and A. M. Stuart. Ensemble Kalman methods with constraints. *Inverse Probl.*, 35(9):095007, 2019.
- [3] J. L. Anderson. An Ensemble Adjustment Kalman Filter for Data Assimilation. *Monthly Weather Review*, 129(12):2884–2903, 2001.
- [4] D. Bloemker, C. Schillings, and P. Wacker. A strongly convergent numerical scheme from ensemble Kalman inversion. *SIAM J. Numer. Anal.*, 56(4):2537–2562, 2018.
- [5] D. Bloemker, C. Schillings, P. Wacker, and S. Weissman. Well Posedness and Convergence Analysis of the Ensemble Kalman Inversion. *Inverse Probl.*, 35(8), 2019.
- [6] J. A. Carrillo, M. Fornasier, G. Toscani, and F. Vecil. *Mathematical Modeling of Collective Behavior in Socio-Economic and Life Sciences*, chapter Particle, kinetic, and hydrodynamic models of swarming, pages 297–336. Modeling and Simulation in Science, Engineering and Technology. Birkhäuser Boston, 2010.
- [7] J. A. Carrillo and U. Vaes. Wasserstein stability estimates for covariance-preconditioned Fokker-Planck equations. Preprint arXiv:1910.07555, 2019.
- [8] N. K. Chada, A. M. Stuart, and X. T. Tong. Tikhonov regularization within ensemble Kalman inversion. *SIAM J. Numer. Anal.*, 58(2):1263–1294, 2020.
- [9] Z. Ding and Q. Li. Ensemble Kalman Inversion: mean-field limit and convergence analysis. Preprint arXiv:1908.05575, 2019.
- [10] G. Evensen. Sequential data assimilation with a nonlinear quasi-geostrophic model using Monte Carlo methods to forecast error statistics. *J. Geophys. Res.*, 99:10143–10162, 1994.
- [11] G. Evensen and P. J. Van Leeuwen. Assimilation of geosat altimeter data for the agulhas current using the ensemble Kalman filter with a quasi-geostrophic model. *Monthly Weather*, 128:85–96, 1996.
- [12] A. Garbuno-Inigo, F. Hoffmann, W. Li, and A. M. Stuart. Interacting Langevin Diffusions: Gradient Structure and Ensemble Kalman Sampler. *SIAM J. Appl. Dyn. Syst.*, 19(1):412–441, 2020.
- [13] John Guckenheimer and Philip Holmes. *Nonlinear oscillations, dynamical systems, and bifurcations of vector fields*, volume 42. Springer Science & Business Media, 2013.
- [14] S.-Y. Ha and E. Tadmor. From particle to kinetic and hydrodynamic descriptions of flocking. *Kinet. Relat. Models*, 3(1):415–435, 2008.
- [15] E. Haber, F. Lucka, and L. Ruthotto. Never look back - A modified EnKF method and its application to the training of neural networks without back propagation. Preprint arXiv:1805.08034, 2018.

- [16] M. Herty and G. Visconti. Kinetic methods for inverse problems. *Kinet. Relat. Models*, 12(5):1109–1130, 2019.
- [17] M. Herty and G. Visconti. Continuous limits for constrained ensemble Kalman filter. *Inverse Probl.*, 2020.
- [18] M. Iglesias, K. Law, and A. M. Stuart. Ensemble Kalman methods for inverse problems. *Inverse Probl.*, 29(4):045001, 2013.
- [19] T. Janjić, D. McLaughlin, S. E. Cohn, and M. Verlaan. Conservation of mass and preservation of positivity with ensemble-type Kalman filter algorithms. *Monthly Weather Review*, 142(2):755–773, 2014.
- [20] N. B. Kovachki and A. M. Stuart. Ensemble Kalman inversion: a derivative-free technique for machine learning tasks. *Inverse Probl.*, 35(9):095005, 2019.
- [21] L. Pareschi and G. Toscani. *Interacting Multiagent Systems. Kinetic equations and Monte Carlo methods*. Oxford University Press, 2013.
- [22] C. Schillings and A. M. Stuart. Analysis of the Ensemble Kalman Filter for Inverse Problems. *SIAM J. Numer. Anal.*, 55(3):1264–1290, 2017.
- [23] C. Schillings and A. M. Stuart. Convergence analysis of ensemble Kalman inversion: the linear, noisy case. *Appl. Anal.*, 97(1):107–123, 2018.
- [24] M. Schwenzer, G. Visconti, M. Ay, T. Bergs, M. Herty, and D. Abel. Identifying trending coefficients with an ensemble Kalman filter. Preprint arXiv:2001.10861, 2019.
- [25] B. O. S. Teixeira, L. A. B. Târres, L. A. Aguirre, and D. S. Bernstein. On unscented Kalman filtering with state interval constraints. *J. Process Contr.*, 20(1):45–57, 2010.
- [26] X. T. Tong, A. J. Majda, and D. Kelly. Nonlinear stability of the ensemble Kalman filter with adaptive covariance inflation. *Commun. Math. Sci.*, 14(5):1283–1313, 2016.
- [27] G. Toscani. Kinetic models of opinion formation. *Commun. Math. Sci.*, 4(3):481–496, 2006.
- [28] X.-L. Zhang, C. Michelén-Ströfer, and H. Xiao. Regularized ensemble Kalman methods for inverse problems. Preprint arXiv:1910.01292, 2019.